Applied Clay Science 181 (2019) 105207

Contents lists available at ScienceDirect

Applied Clay Science

journal homepage: www.elsevier.com/locate/clay

Research Paper

Transformation of boehmite into 2:1 type layered aluminosilicates with different layer charges under hydrothermal conditions

Shangying Li[a,b], Hongping He[a,b,*], Qi Tao[a], Yunfei Xi[c], Aiqing Chen[a,b], Shichao Ji[a,b], Chaoqun Zhang[a,b], Yiping Yang[a,b], Jianxi Zhu[a]

[a] Key Laboratory of Mineralogy and Metallogeny, Chinese Academy of Sciences & Guangdong Provincial Key Laboratory of Mineral Physics and Materials, Guangzhou Institute of Geochemistry, Guangzhou 510640, China
[b] University of Chinese Academy of Sciences, Beijing 100049, China
[c] School of Earth, Environmental and Biological Sciences, Queensland University of Technology (QUT), 2 George Street, Brisbane, Queensland 4001, Australia

ARTICLE INFO

Keywords:
Boehmite
Beidellite
2:1 type layered aluminosilicates
Layer charge
Transformation

ABSTRACT

In this study, beidellite, paragonite and other 2:1 type layered aluminosilicates with high layer charges (2:1 type LA-HLC) were synthesized under hydrothermal conditions by using boehmite as a precursor. The concentrations of dissolved Al from boehmite precursor had important effects on the mineral components of the hydrothermal products and the layer charge density of the resultant minerals. A combination of 2:1 type LA-HLC, paragonite, and minor beidellite formed at a relatively high concentration of dissolved Al, while beidellite with a small amount of 2:1 type LA-HLC was produced at a low concentration of dissolved Al. The resultant 2:1 type LA-HLC exhibited poor swelling ability when treated with ethylene glycol. A solid-state transformation mechanism was proposed for the transformation based on the HRTEM images and EDS analyses, which showed that lattice fringes representing (001) faces of 2:1 type layered aluminosilicates (2:1 type LA) were parallel to the (020) direction of boehmite. The successful transformation of boehmite into 2:1 type LA provides insights to well understand the formation of 2:1 type LA in geological processes and offer a facile preparation approach for the synthesis of 2:1 type LA with different layer charges.

1. Introduction

Layered aluminosilicates (LA) are ubiquitous in various natural environments on the Earth surface. As a family of important natural materials, they are widely utilized in ceramics, oil drilling, paper industries, environmental remediation and pharmaceutical industry (Konta, 1995; Murray and Kogel, 2005; Khodja et al., 2010; Viseras et al., 2010; Zhu et al., 2016). Specifically, 2:1 type LA with high layer charges (2:1 type LA-HLC) are promising materials to remove radioactive ions (Noh et al., 2013; Pavon et al., 2013). Synthetic layered silicates have displayed widespread applications due to high purities and adjustable chemical compositions (Zhang et al., 2010).

It is well known that aluminum minerals (e.g., boehmite, gibbsite, and bayerite) in bauxite always coexist with clay minerals (e.g., kaolinite, beidellite, and illite). Previous studies demonstrated that layered silicates could be converted into aluminum minerals during chemical weathering processes, with aluminum retention as well as silicon and alkali metals elements removal (Wolfenden, 1965; Bird et al., 1989; Yu et al., 2014). Meanwhile, an inverse conversion process, the transformation of gibbsite or bayerite into 2:1 type LA, was also achievable under hydrothermal condition (Granquist and Pollack, 1967; Granquist et al., 1972). Such formation mechanism for clay minerals was also found in nature (Mcmurtry and Yeh, 1981; Marumo and Hattori, 1999; Mas et al., 2006). This means that, when aluminum minerals encounter with silicon-rich geological fluids and undergo hydrothermal alteration, they can be transformed into clay minerals in geological processes, namely, 'resilicification' of aluminum minerals. However, the factors controlling the layer charges of 2:1 type LA in these processes are not clear yet. The transformation from aluminum minerals to 2:1 type LA and the mechanism involved is of importance for understanding the genesis of natural clay minerals and synthesis of 2:1 type LA with the unique property.

So far, two transformation mechanisms of LA have been proposed, i.e., dissolution-recrystallization and solid-state transformation. However, the definitions of these two mechanisms are not unambiguous as reported in previous studies (Srodon, 1980; Srodon and Eberl, 1984; Inoue et al., 1988; Delvaux et al., 1989; Grubb et al., 1991; Lindgreen et al., 1991; Buatier et al., 1993; BettisonVarga and Mackinnon, 1997;

* Corresponding author at: Guangzhou Institute of Geochemistry, Chinese Academy of Sciences, No. 511 Kehua Street, Tianhe District, Guangzhou 510640, China.
E-mail address: hehp@gig.ac.cn (H. He).

https://doi.org/10.1016/j.clay.2019.105207
Received 6 February 2019; Received in revised form 4 July 2019; Accepted 5 July 2019
Available online 16 July 2019
0169-1317/

Amouric and Olives, 1998; Cuadros and Altaner, 1998; Murakami et al., 1999; Dudek et al., 2006;). To clarify these two transformation mechanisms, in our view, the process of complete dissolution of original mineral and subsequent recrystallization of another new phase is identified as dissolution-recrystallization. And solid-state transformation means, at least, part of precursor mineral's structural unit (e.g., tetrahedral or octahedral sheet) is kept in the solid state but partial dissolution (e.g., dissolution of Si—O tetrahedral sheet in kaolinization of smectites) maybe occurs during the transformation process.

The main aim of this study is to investigate the possibility for the transformation of aluminum minerals to 2:1 type LA with different layer charges and elucidate the transformation mechanism involved. Hence, boehmite was used as a precursor mineral and $Na_2SiO_3{\cdot}9H_2O$ as the source of silicon in the hydrothermal experiments. The obtained hydrothermal products were systematically characterized by X-ray diffraction (XRD), solid-state magic-angle-spinning nuclear magnetic resonance spectroscopy (MAS NMR), inductively coupled plasma mass spectrometry (ICP-MS), Fourier transform infrared spectroscopy (FTIR), scanning electron microscopy (SEM), and transmission electron microscopy (TEM).

2. Experiments

2.1. Preparation of precursor mineral and hydrothermal experiments

Commercial alumina trihydrate ($Al(OH)_3$) was purchased from Fuchen Chemical Factory (Tianjin), which belonges to gibbsite phase based on the XRD pattern (not shown). And sodium metasilicate ($Na_2SiO_3{\cdot}9H_2O$) of analytical grade was purchased from Aladdin industrial corporation (Shanghai, China).

Boehmite was prepared from gibbsite (Trolard and Tardy, 1987). After calcination at the temperature of 300 °C and ambient pressure for 24 h in a muffle furnace, the XRD pattern showed that gibbsite was completely transformed into boehmite (Fig. 1). The hydrothermal experiments were conducted as follows: 17.052 g of $Na_2SiO_3{\cdot}9H_2O$, as the source of silicon, was dissolved into 100 mL of deionized water and the pH of the solution was adjusted to 8 using 6 M HCl. Then, 1.800 g of the prepared boehmite was added into the solution under vigorous stirring. Finally, the obtained mixtures were put in 250 mL autoclaves separately and maintained at 350 °C with different time intervals. The resultant products were firstly centrifuged at 4000 r/min for 5 min and the supernatants were kept for Al concentration determination, and the sediments were washed several times with deionized water in order to remove excess sodium chloride. All the obtained samples were dried at 80 °C (He et al., 2014), and were marked as Boe-X, in which Boe and X stood for boehmite and duration time at 350 °C (e.g., 1d = 1 day and 1w = 1 week), respectively.

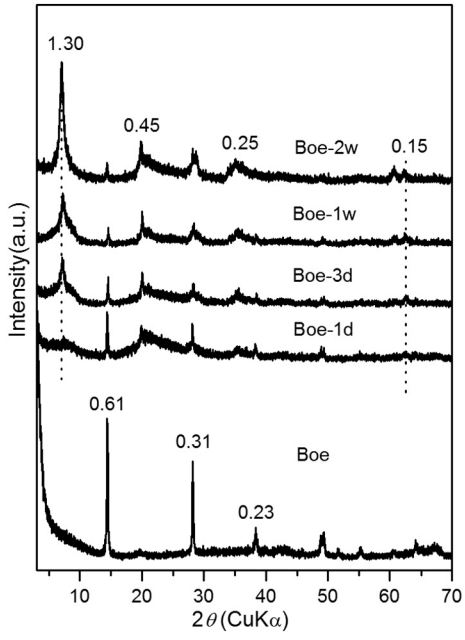

Fig. 1. XRD patterns of precursor boehmite and hydrothermal products after different duration time. Boehmite (Boe); The hydrothermal product after one day (Boe-1d), three days (Boe-3d), one week (Boe-1w) and two weeks (Boe-2w). All spacing unit is nanometer (nm).

2.2. Characterization methods

2.2.1. X-ray diffraction (XRD)

XRD analyses were performed using a Bruker D8 Advance diffractometer with Ni-filtered CuKα radiation (λ = 0.154 nm, 40 kV and 40 mA) (Guangzhou Institute of Geochemistry (GIG), Chinese Academy of Sciences (CAS)). XRD patterns of randomly oriented samples were collected between 3° and 70° (2θ) at a scanning rate of 3° (2θ) min^{-1}. To clearly exhibit the characteristic (001) reflections of 2:1 type LA, air-dry oriented samples of Boe-3d, Boe-1w, and Boe-2w were prepared by carefully pipetting dispersions onto glass slides and allowed to dry slowly at ambient temperature. Glycolated samples were prepared by saturating air-dry oriented samples in ethylene glycol atmosphere at 60 °C for 12 h to test the swelling abilities (Kloprogge et al., 1990; Kloprogge et al., 1993). Air-dry and glycolated samples were also investigated using the same diffractometer and parameters mentioned above. The peak decomposition analyses of air-dry and glycolated samples were undertaken using a Jade software package. The variables of height, 2-theta, full width at half maxima (FWHM) were chosen to refine. And the positions and relatively symmetric shapes of reflections obtained until the residual error of fit kept unchanged.

2.2.2. Magic-angle-spinning nuclear magnetic resonance spectroscopy (MAS NMR)

^{29}Si MAS NMR spectral measurements were performed on a Bruker AVANCE III 600 spectrometer at a resonance frequency of 119.2 MHz (High magnetic field laboratory, CAS). ^{29}Si MAS NMR spectra with high-power proton decoupling were recorded on a 4 mm probe with a spinning rate of 12 kHz, a π/4 pulse length of 2.6 μs, and a recycle delay of 80 s. The chemical shifts of ^{29}Si were referenced to tetramethylsilane (TMS). In order to calculate the Si/Al ratios in the tetrahedral sheets of layered aluminosilicates (Sanz and Serratosa, 1984), peak component analysis was undertaken using a Gauss–Lorentz cross-product function applied by the PEAKFIT software package. The positions and areas of peaks were obtained until the squared correlation coefficients (r^2) were more than 0.995 and the iteration values were almost a constant (He et al., 2014).

2.2.3. Inductively coupled plasma mass spectrometry (ICP-MS)

Due to the possible dissolution of Al from boehmite precursor in the hydrothermal experiments at 350 °C (Trolard and Tardy, 1987), the Al concentrations in the supernatants after hydrothermal experiments were determined using Thermoscientific iCAP Qc inductively coupled plasma mass spectrometer (ICP-MS) (GIG, CAS). Al concentration in each supernatant was examined five times and then obtain the average value. The relative standard deviations (RSD %) of concentration values of samples were not more than 1.2%. In this study, the complexation of Al with OH^- ligand in solution was not considered.

2.2.4. Fourier transform infrared spectroscopy (FTIR)

The FTIR spectra were recorded on a Bruker Vertex-70 Fourier transform infrared spectrometer (GIG, CAS) using KBr pressed disk technique. Each KBr pellet was prepared by mixing 0.9 mg of sample with 80 mg of KBr, and ground well in an agate mortar for 15 min. The mixtures were pressed for 5 min at 10 kbars and heated under a lamp

for 3 min to reduce adsorbed water before FTIR measurements. The spectra were collected in the 4000–400 cm^{-1} range with 64 scans and a resolution of 4 cm^{-1}.

2.2.5. Scanning electron microscopy (SEM)

Scanning electron microscopy (SEM) images were obtained on a field emission scanning electron microscopy equipped at 1.5 kV accelerating voltage and at a working distance (WD) of 2.9 mm (FESEM, SU8010, Hitachi, Japan) (GIG, CAS). Particles were analyzed with an Apollo X-SDD detector, live time of 40 s and a spot size of ~10 nm. Dried sample powders were glued evenly onto conductive adhesive tapes for SEM observation.

2.2.6. Transmission electron microscopy (TEM)

TEM observations were performed on an FEI Talos F200S microscope equipped with an X-ray energy-dispersive detector. The specimen was prepared by adding the hydrothermal product in ethanol and ultrasonically dispersed for 5 min. A droplet of resultant dispersion was deposited onto a porous carbon film supported by a copper grid. Then, ethanol was evaporated at room temperature. To obtain HRTEM images, a small amount of hydrothermal product was embedded in epoxy resin and dried to solidify. Ultrathin sections with a thickness of approximately 75 nm were prepared with a diamond knife by operating on a Lecia EM UC7 ultramicrotome.

3. Results and discussion

3.1. XRD patterns

In the XRD patterns of randomly oriented samples (Fig. 1), the beidellite phase was identified by the reflections with *d*-values at ~1.30, 0.45, 0.25, and 0.15 nm, corresponding to (001), (0211), (1320) and (060) reflections, respectively (Fig. 1). The (001) reflection intensity of 2:1 type LA increased with the increase of reaction time, reflecting an increase of crystallinity or/and content of neoformed 2:1 type LA (He et al., 2014). The (0211) reflection of 2:1 type LA was well displayed while no obvious (001) reflection was observed for sample Boe-1d (Fig. 1). Since these two reflections correspond to crystal growth in *a-b* plane and layer stacking along the *c* axis of 2:1 type LA, respectively, the XRD pattern of Boe-1 implied that the crystal growth in *a-b* plane was readily to happen, followed by layer stacking.

Residual boehmite precursor in all hydrothermal products was still detectable in XRD patterns of randomly oriented samples, as indicated by the occurrence of the characteristic (020) reflection at 0.61 nm (Fig. 1). Its reflection intensities gradually decreased with the increase of reaction time, reflecting the consumption of boehmite during the hydrothermal processes. The humps at 20–30° (2θ) in the XRD patterns may correspond to the formation of amorphous silica in the hydrothermal products (Fig. 1).

As shown by the XRD patterns of both the air-dry and glycolated oriented samples (Fig. 2), the (001) reflections were obviously asymmetric. This suggested that hydrothermal products were a mixture of diverse minerals. To identify the mineral components in the products, deconvolutions of the reflections were conducted and the results were also shown in Fig. 2. Three reflections with *d*-value of approximately 1.24, 1.12, and 0.97 nm, respectively, occurred in the sample Boe-3d, while two reflections around 1.25 and 1.12 or 1.18 nm appeared in the sample Boe-1w and Boe-2w (Fig. 2a). However, after ethylene glycol treatment, the broad reflection of Boe-3d was proposed to be composed of four reflections at 1.55, 1.33, 1.12 and 0.97 nm, respectively. Among them, The 1.55 nm reflection could correspond to beidellite-like phase (Fig. 2b), which exhibited swelling ability. The reflection at 1.33 nm was assigned to 2:1 type LA-HLC, with the poor swelling ability (Cuadros et al., 2015). Note that two reflections at ca. 0.97 and 1.12 nm occurred in both the samples before and after ethylene glycol treatment, which maybe correspond to the non-swelling mica-like minerals with different layer charge density (Pazos et al., 2012). The phase with *d*-value of 0.97 nm could be attributed to the formation of paragonite (Granquist and Pollack, 1967), while the one with *d*-value of 1.12 nm, most possibly, corresponded to a paragonite-like phase with relatively low layer charge density, in comparison to that of paragonite. In other words, in the case of paragonite, the interlayer sodium ions are naked (without any hydrated water molecules) while for the paragonite-like phase (with *d*-value of 1.12 nm), the interlayer sodium ions are partially hydrated (with one water pseudo-monolayer) (Pazos et al., 2012). Both the XRD patterns of Boe-1w and Boe-2w, before and after ethylene glycol treatment, are similar (Fig. 2b). Before the treatment, the prominent reflection occurred at ca. 1.25 nm while a shoulder centered at ca. 1.12 or 1.18 nm. However, after the ethylene glycol treatment, the prominent reflection shifted to around 1.70 nm, displaying excellent swelling property, while a slight increase of the basal spacing occurred in the phase corresponding to the reflection at ca. 1.39 or 1.35 nm. We attributed the former to neoformed beidellite and the latter to 2:1 type LA-HLC. Here, we can find that an obvious mineral evolution (mainly related to the layer charge density) occurred in the hydrothermal experiments with an increase of duration time, i.e., 2:1 type LA-HLC and paragonite, with minor beidellite, were the dominant mineral components of the products formed at the initial stage of hydrothermal experiments, while beidellite and a small amount of 2:1 type LA-HLC were readily produced at the late stage.

3.2. ^{29}Si MAS NMR spectra and ICP-MS

To get a better understanding of isomorphous substitution of Al^{3+} for Si^{4+} in the tetrahedral sheets of 2:1 type LA, solid-state ^{29}Si MAS NMR spectra were performed on all hydrothermal products, and the obtained spectra displayed five distinct ^{29}Si signals (Fig. 3). The signals recorded at approximately −80, −86 and − 91 ppm correspond to Q^3Si(2Al), Q^3Si(1Al), and Q^3Si(0Al) units, respectively (Sanz and Serratosa, 1984; He et al., 2003). Here, Q^3Si(nAl) refers to one Si − O tetrahedron linked with three neighboring tetrahedrons in the tetrahedral sheet, and n of the three tetrahedra are occupied by Al via $Al^{3+} \rightarrow Si^{4+}$. In addition, two ^{29}Si signals at around −101 and − 111 ppm, corresponding to Q^4Si (Mackenzie et al., 1987; Bouna et al., 2012; Pomakhina et al., 2012), which should be attributed to amorphous silica formed from the condensation of hydrolyzed metasilicate during the hydrothermal reaction. This was consistent with the existence of amorphous silica in the XRD patterns (Fig. 1).

It is well known the isomorphous substitution of Al^{3+} for Si^{4+} in the tetrahedral sheets of 2:1 type LA gives the layers net negative charges. This part charges will be compensated by interlayer cations. Accordingly, the ^{29}Si NMR spectra could provide valuable information to calculate the Si/Al ratios in the tetrahedral sheets of 2:1 type LA according to the following expression:

$$(\mathrm{Si/Al})\mathrm{NMR} = \sum_{n=0}^{3} \mathrm{ISi(nAl)} / \sum_{n=0}^{3} (n/3)/\mathrm{ISi(nAl)}$$

where ISi(nAl) is the integrated area of the corresponding signal (Sanz and Serratosa, 1984). The layer charges of 2:1 type LA for the general formula of $(M^+)_x(Si_{4-x}Al_x)Al_2O_{10}(OH)_2{\cdot}nH_2O$ can be estimated according to the calculated Si/Al ratio values in the tetrahedral sheets because they were dominantly produced by the isomorphous substitution of Al^{3+} for Si^{4+} in the tetrahedral sheets.

It can be found that the calculated layer charges of 2:1 type LA in sample Boe-1w and Boe-2w were higher than the that of beidellite (~0.2 − ~0.6 per half unit cell (/$O_{10}(OH)_2$)) (Table 1), indicating that 2:1 type LA-HLC, in comparison to beidellite, were included in the hydrothermal products. It is noteworthy that the estimated layer charge in sample Boe-3d was relatively high, suggesting the appearances of 2:1 type LA-HLC or/and paragonite. It is well known that the swelling ability of 2:1 type LA is closely related to their layer charge density.

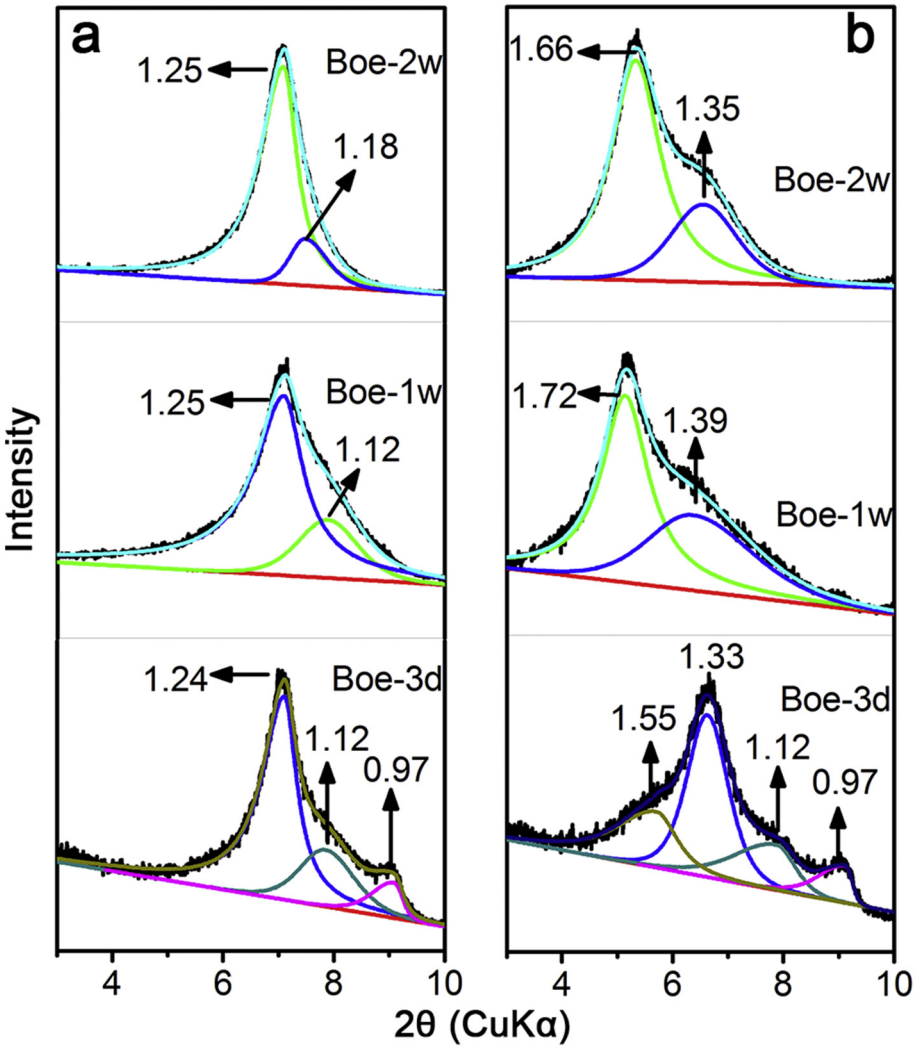

Fig. 2. XRD patterns of air-dry (a) and glycolated (b) samples. The hydrothermal product after three days (Boe-3d), one week (Boe-1w) and two weeks (Boe-2w). All spacing unit is nanometer (nm).

Hence, these results were consistent with the mineral constituents in the hydrothermal products deduced from the corresponding XRD patterns (Fig. 2b), i.e., samples Boe-1w and Boe-2w were composed of beidellite, 2:1 type LA-HLC while sample Boe-3d contained 2:1 type LA-HLC, paragonite, and beidellite.

To elucidate the relationship between the dissolved Al concentration and the layer charge density of the resultant 2:1 type LA, the dissolved Al concentrations in the supernatants were measured and shown in Table 1. Although the detected Al concentrations did not exactly represent the amounts of Al dissolved from boehmite to some extent, they kept the traces of Al dissolved from boehmite and reflected the change of the dissolved Al concentration during the conversion. The difference of the dissolved Al concentrations in the supernatant solutions was caused by the dissolution of different boehmite particles in the reaction processes, which were probably related to the boehmite particle sizes the interaction between boehmite and additive silicon.

It can be found that, at the initial stage of the transformation process, the concentration of the dissolved Al in the supernatant was relatively high, and a combination of 2:1 type LA-HLC, paragonite, and minor beidellite formed in sample Boe-3d. However, with the transformation reaction going on, the concentration of the dissolved Al decreased, and a combination of beidellite and a small amount of 2:1 type LA-HLC readily occurred in the samples Boe-1w and Boe-2w. As proposed by the recent studies (He et al., 2017; Ji et al., 2018), the dissolved Al ions from precursor minerals preferred to occupying the tetrahedral sites by the isomorphous substitution of Al^{3+} for Si^{4+} during these transformation processes. Hence, based on the assumption that Al ions from solutions preferred to occupy in tetrahedral sites of the neoformed 2:1 type LA and their octahedral Al inherit from the boehmite precursor via solid-state transformation, the dissolved Al from precursor boehmite had important effects on the neoformed 2:1 type LA components and their layer charge density as well.

3.3. FTIR spectra

The chemical structures of boehmite precursor and synthetic 2:1 type LA in the hydrothermal products were well identified in FTIR spectra (Fig. 4). Two well-resolved absorption bands at 3293 and 3098 cm^{-1} were recorded and assigned to the Al–OH stretching vibrations of boehmite (Ram, 2001; Boumaza et al., 2009). Both bands became weaker with the increase of hydrothermal treatment time, reflecting a decrease of the boehmite content. The vibrations at 1075 and 730 cm^{-1} corresponded to the Al—O stretching and bending modes of boehmite, respectively (Ram, 2001). Meanwhile, surface adsorbed water and interlayer water in beidellite displayed –OH stretching and bending vibrations at around 3445 and 1634 cm^{-1}, respectively (Kloprogge, 2006). The obvious absorption band at 3628 cm^{-1} corresponded to Al–OH stretching vibration of 2:1 type LA, which is very

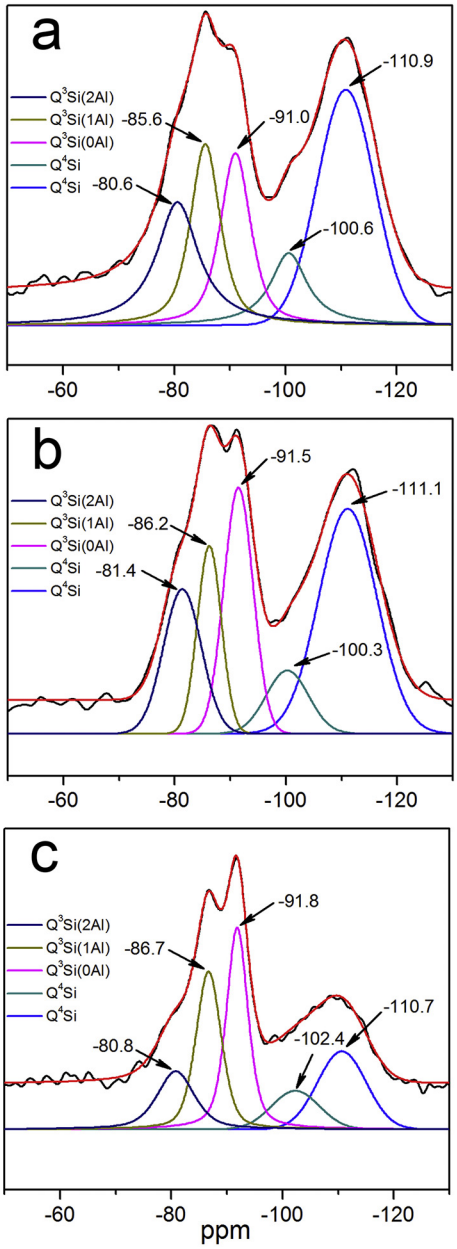

Fig. 3. ^{29}Si MAS NMR spectra of hydrothermal products after different duration time. (a) The hydrothermal product after three days (Boe-3d); (b) one week (Boe-1w); (c) two weeks (Boe-2w).

Table 1
Al concentrations in the supernatant solutions of hydrothermal products after different duration time as well as Si/Al ratios in the tetrahedral sheets and their estimated layer charges of 2:1 type LA in hydrothermal products. RSD denoted the relative standard deviations of Al concentration values.

Samples	Al concentrations (ppm) (RSD %)	Si/Al ratios	Layer charges
Boe-3d	5.011 (0.8)	2.903	1.025
Boe-1w	0.582 (1.1)	3.557	0.878
Boe-2w	1.113 (1.2)	3.787	0.836

close to that of natural beidellite (van der Marel and Beutelspacher, 1976), but lower than those reported in previous studies (Kloprogge et al., 1990; Kloprogge, 2006). This might be influenced by the high layer charges densities of 2:1 type LA (Kloprogge et al., 2000). The vibration at 782 cm^{-1} could be attributed to the Al–OH bending mode

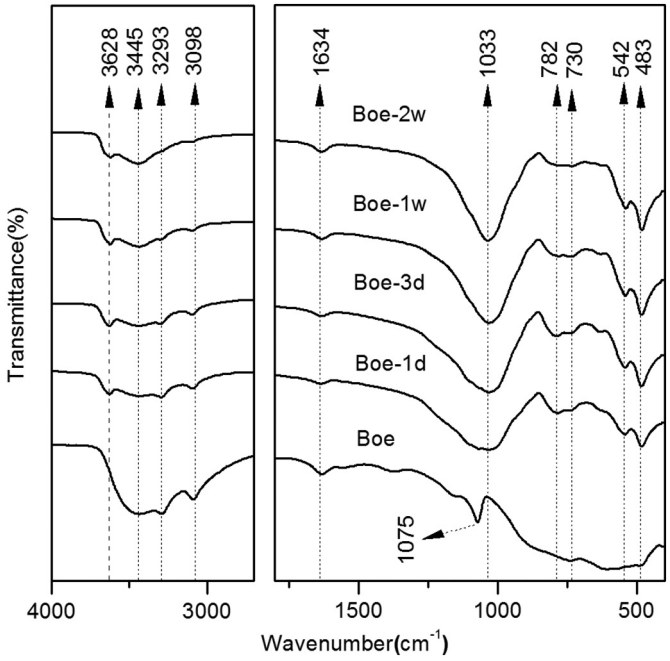

Fig. 4. FTIR spectra of precursor boehmite and hydrothermal products after different duration time. Boehmite (Boe); The hydrothermal product after one day (Boe-1d), three days (Boe-3d), one week (Boe-1w) and two weeks (Boe-2w).

for 2:1 type LA.

The absorption band at 1033 cm^{-1} was assigned to Si–O–Si stretching vibration, which became gradually stronger from sample Boe-1d to Boe-2w, and its bending vibration occurred at 483 cm^{-1}. The band at 542 cm^{-1} could be related to Si–O–Al bending vibration of 2:1 type LA (Granquist and Pollack, 1967; Bishop et al., 2011). Notably, both the Al–OH stretching vibration at 3628 cm^{-1} and the Si–O–Al bending vibration at 542 cm^{-1} were displayed in sample Boe-1d, indicating the formation of 2:1 type LA. This was consistent with the XRD result (Fig. 1).

3.4. SEM observations

As shown by SEM images (Fig. 5a), some boehmite particles were in micrometer size and displayed straight boundary, while the other small particles in nanoscale size exhibited irregular boundaries. After one-day hydrothermal treatment, significant morphology changes of these particles could be observed. Some small foliated grains appeared, suggesting the formation of new mineral phases (Fig. 5b). In addition, dissolution pits (shown as the inset in Fig. 5b) appeared on the surface of some particles, which suggested the local dissolution of boehmite. There were more grains with foliated morphology in the images of products of Boe-3d and Boe-1w, corresponding to an increase of neoformed LA in the hydrothermal products (Fig. 5c and d). Notably, different morphologies such as granular-like particles with rough surfaces and flake-like aggregates were observed simultaneously in the SEM image of Boe-1w (Fig. 5d). EDS analyses indicated that the Si/Al ratio of spot 1 was 1.91 for flake-like aggregates, close to that of 2:1 type LA, while that of spot 2 was 17.52, indicating amorphous silica precipitated on the particle (Fig. 5d). The SEM image of sample Boe-2w showed great amounts of aggregates with corrugated and scrolled morphologies (Fig. 5e), which were the characteristic morphology of smectite and related layered silicates by the SEM observations (Yanagisawa et al., 1995; Chen et al., 2013). Some particles with rod-like morphology were also observed (Fig. 5f), which probably were residual boehmite nanofibres after hydrothermal treatment (Nagai et al., 2012).

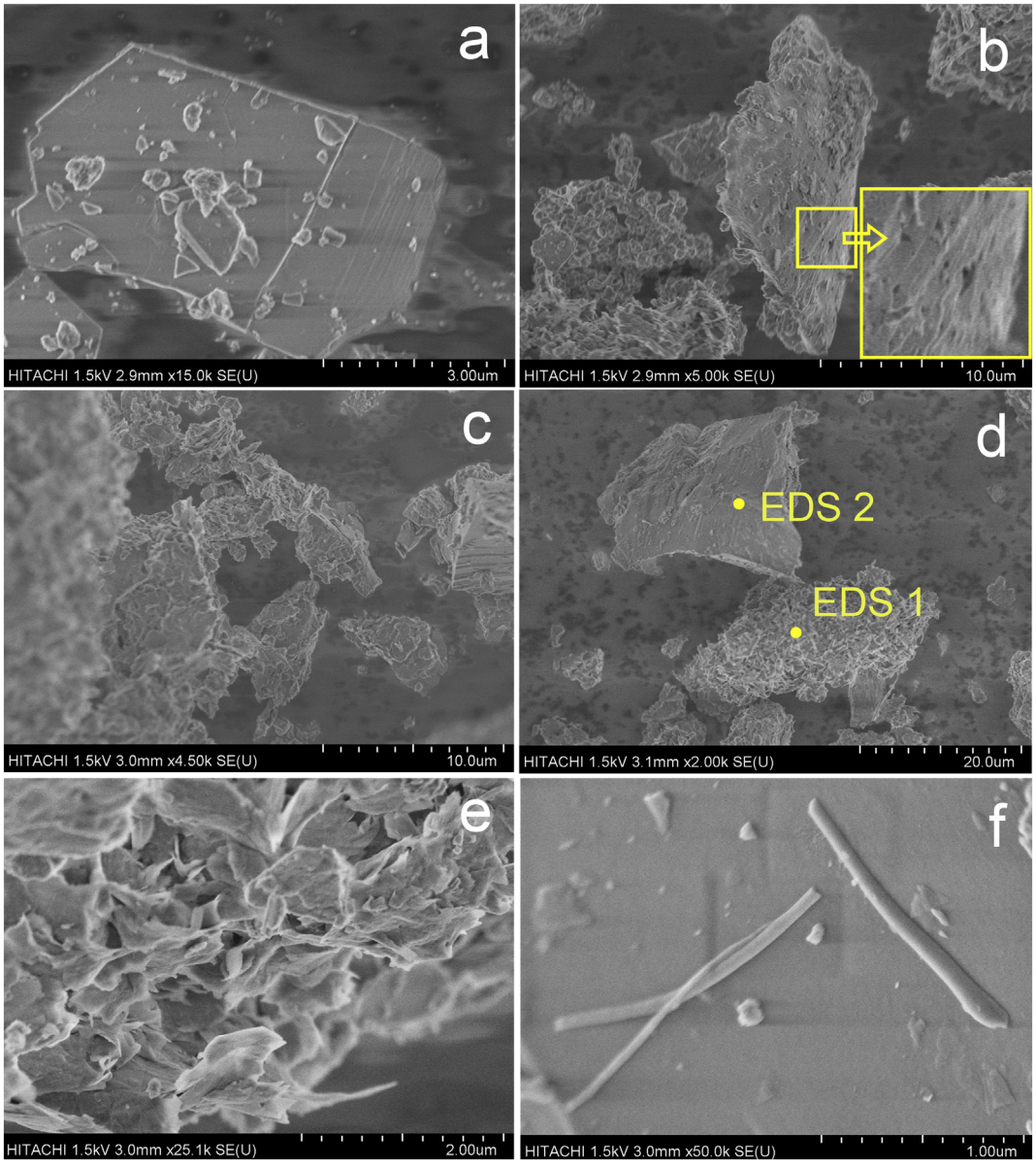

Fig. 5. SEM images of precursor boehmite and hydrothermal products after different duration time. (a) Boehmite (Boe); (b) The hydrothermal product after one day (Boe-1d); (c) three days (Boe-3d); (d) one week (Boe-1w); (e-f) two weeks (Boe-2w).

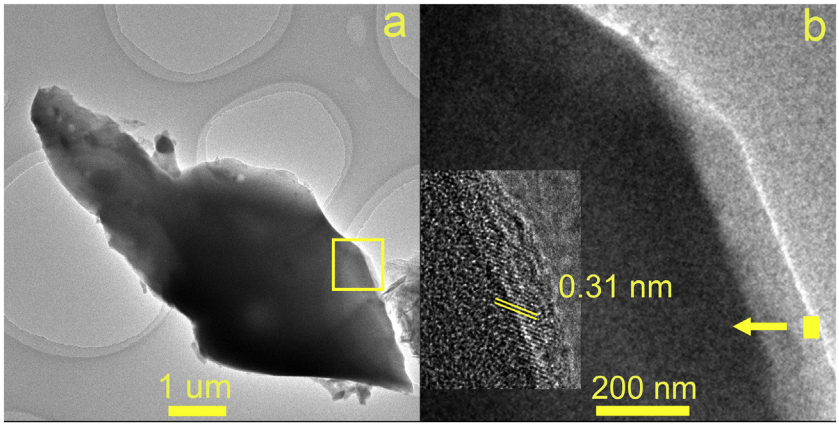

Fig. 6. TEM images of the particles in the hydrothermal product after one day (Boe-1d) (a). Image b was the magnification of region surrounded by the yellow rectangle in image a. The Insert image in the bottom left corner in image b was the HRTEM image of the local edge indicated by a yellow solid rectangle. The specimen was prepared by ethanol dispersion method. (For interpretation of the references to colour in this figure legend, the reader is referred to the web version of this article.)

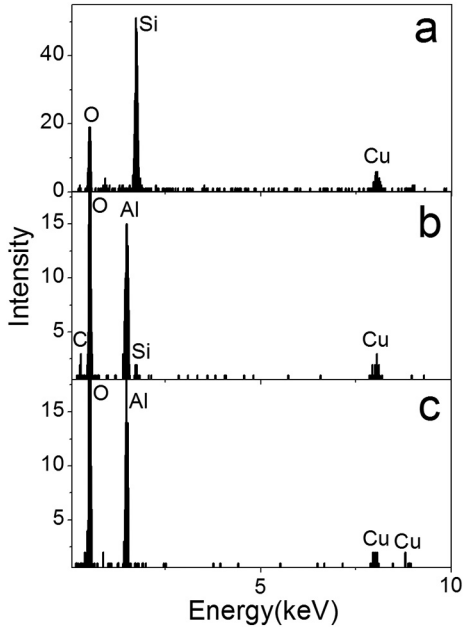

Fig. 7. EDS spectra of particle or nanodomains in the hydrothermal product after one day (Boe-1d). (a) The particle in Fig. 6b; (b) EDS 1 marked by a yellow circle in Fig. 8; (c) EDS 2 marked by a yellow circle in Fig. 8. (For interpretation of the references to colour in this figure legend, the reader is referred to the web version of this article.)

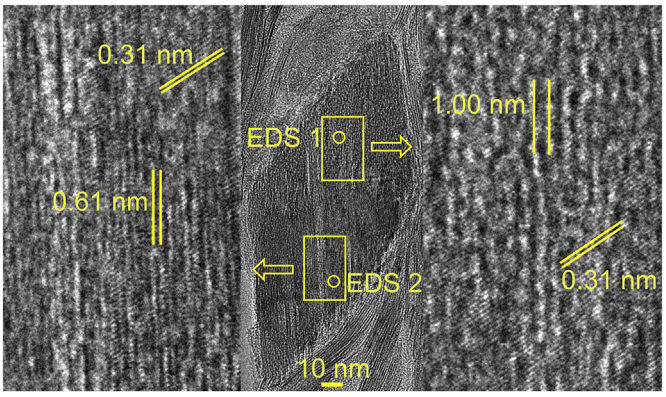

Fig. 8. TEM images (in the middle) of the hydrothermal product after one day (Boe-1d). Images on the left and right were the HRTEM images marked by two yellow rectangles, respectively. The specimen was prepared by the ultrathin-section method. (For interpretation of the references to colour in this figure legend, the reader is referred to the web version of this article.)

3.5. TEM observations

The XRD pattern and FTIR spectrum indicated that 2:1 type LA and boehmite coexisted in the sample Boe-1d. The particle with euhedral and straight edge was found in sample Boe-1d (Fig. 6a), and the lattice fringes in the boundary were with a periodicity of ~0.31 nm (Fig. 6b), consistent with the (120) spacing value of boehmite. However, EDS analysis showed the particle contained significantly high silicon (Fig. 7a). This indicated that some boehmite particles were wrapped by amorphous silica at the initial stage of hydrothermal treatment and then gradually transformed to 2:1 type LA (Granquist et al., 1972).

The lattice fringes with a periodicity of ~1.00 nm corresponded to the layers of 2:1 type LA (Fig. 8). It was difficult to distinguish the paragonite layers from other 2:1 type LA (e.g., beidellite) ones due to the escape of interlayer water by electron beam heating. Fig. 8 showed the coexistence of boehmite with 2:1 type LA within one particle. In detail, lattice fringes with periodicities of ~0.61 and ~0.31 nm corresponded to (020) and (120) faces of boehmite, respectively. And the lattice fringes with a periodicity of ~1.00 nm distributed along the direction of (020) face of boehmite and accompanied lattice fringes with a periodicity of ~0.31 nm in the nanodomain. This indicated that boehmite was partially converted to 2:1 type LA. EDS analysis showed that the nanodomain, in which both 2:1 type LA and boehmite occurred, contained Al and a small amount of Si (Fig. 7b), while boehmite nanodomain contained Al and almost no Si (Fig. 7c). This was consistent with the chemical compositions of boehmite and 2:1 type LA. A solid-state transformation mechanism could be proposed for the transformation of boehmite into 2:1 type LA, since the neoformed 2:1 type LA exhibited a topological inheritance from the boehmite precursor. Possibly, such transformation was induced by the wrapping boehmite with amorphous silica.

4. Conclusions

The present study demonstrated boehmite could be transformed into 2:1 type LA under hydrothermal conditions, most likely, through a solid-state transformation. During the transformation process, hydrolyzed metasilicates attached onto the surface of boehmite to form 2:1 type LA, of which the layers were parallel to the (020) direction of boehmite. However, the dissolved Al from the precursor boehmite strongly affected the layer charge intensity of 2:1 type LA. A combination of 2:1 type LA-HLC, paragonite, and minor beidellite formed when the content of dissolved Al was relatively high in the hydrothermal system, and 2:1 type LA-HLC exhibited poorly swelling ability after ethylene glycol treatment. A combination of beidellite and a small amount of 2:1 type LA-HLC were readily produced under low dissolved Al concentrations. The insights obtained in this study are of high importance for better understanding the transformation between aluminum minerals and layered aluminosilicates and the genesis of clay mineral deposits, as well as for synthesis and application of clay minerals with the unique property.

Acknowledgments

This work was financially supported by National Natural Science Foundation of China (Grant Nos.41530313, 41772039), National Science Fund for Distinguished Young Scholars of China (Grant No.41825003), CAS Key Research Program of Frontier Sciences (Grant No. QYZDJ-SSW-DQC023-1), and the CAS/SAFEA International Partnership Program for Creative Research Teams (Grant No. 20140491534). The authors thanks the editor and the three reviewers for their valuable comments and suggestions.

References

Amouric, M., Olives, J., 1998. Transformation mechanisms and interstratification in conversion of smectite to kaolinite: an HRTEM study. Clay Clay Miner. 46 (5), 521–527.

BettisonVarga, L., Mackinnon, I.D.R., 1997. The role of randomly mixed-layered chlorite/smectite in the transformation of smectite to chlorite. Clay Clay Miner. 45 (4), 506–516.

Bird, M.I., Chivas, A.R., Andrew, A.S., 1989. A stable-isotope study of lateritic bauxites. Geochim. Cosmochim. Acta 53 (6), 1411–1420.

Bishop, J.L., Gates, W.P., Makarewicz, H.D., McKeown, N.K., Hiroi, T., 2011. Reflectance spectroscopy of beidellites and their importance for mars. Clay Clay Miner. 59 (4), 378–399.

Boumaza, A., Favaro, L., Ledion, J., Sattonnay, G., Brubach, J.B., Berthet, P., Huntz, A.M., Roy, P., Tetot, R., 2009. Transition alumina phases induced by heat treatment of boehmite: an X-ray diffraction and infrared spectroscopy study. J. Solid State Chem. 182 (5), 1171–1176.

Bouna, L., Rhouta, B., Daoudi, L., Maury, F., Amjoud, M., Senocq, F., Lafont, M.C., Jada, A., Aghzzaf, A.A., 2012. Mineralogical and physico-chemical characterizations of ferruginous beidellite-rich clay from Agadir basin (Morocco). Clay Clay Miner. 60 (3), 278–290.

Buatier, M.D., Ouyang, K., Sanchez, J.P., 1993. Iron in hydrothermal clays from the Galapagos spreading center mounds-consequences for the clay transition mechanism. Clay Miner. 28 (4), 641–655.

Chen, T., Wang, H.J., Li, T., Zheng, N., 2013. New insights into the formation of diagenetic illite from TEM studies. Am. Mineral. 98 (5–6), 879–887.
Cuadros, J., Altaner, S.P., 1998. Characterization of mixed-layer illite-smectite from bentonites using microscopic, chemical, and X-ray methods: constraints on the smectite-to-illite transformation mechanism. Am. Mineral. 83 (7–8), 762–774.
Cuadros, J., Diaz-Hernandez, J.L., Sanchez-Navas, A., Garcia-Casco, A., 2015. Role of clay minerals in the formation of atmospheric aggregates of Saharan dust. Atmos. Environ. 120, 160–172.
Delvaux, B., Mestdagh, M.M., Vielvoye, L., Herbillon, A.J., 1989. XRD, IR and ESR study of experimental alteration of Al-nontronite into mixed-layer kaolinite smectite. Clay Miner. 24 (4), 617–630.
Dudek, T., Cuadros, J., Fiore, S., 2006. Interstratified kaolinite-smectite: Nature of the layers and mechanism of smectite kaolinization. Am. Mineral. 91 (1), 159–170.
Granquist, W.T., Pollack, S.S., 1967. Clay mineral synthesis. 2. A randomly interstratified aluminian montmorillonoid. Am. Mineral. 52 (1–2), 212.
Granquist, W.T., Hoffman, G.W., Boteler, R.C., 1972. Clay mineral synthesis. 3. Rapid hydrothermal crystallization of an aluminum smectite. Clay Clay Miner. 20 (5), 323.
Grubb, S.M.B., Peacor, D.R., Jiang, W.T., 1991. Transmission electron-microscope observations of illite polytypism. Clay Clay Miner. 39 (5), 540–550.
He, H.P., Guo, J.G., Zhu, J.X., Hu, C., 2003. ^{29}Si and ^{27}Al MAS NMR study of the thermal transformations of kaolinite from North China. Clay Miner. 38 (4), 551–559.
He, H.P., Li, T., Tao, Q., Chen, T.H., Zhang, D., Zhu, J.X., Yuan, P., Zhu, R.L., 2014. Aluminum ion occupancy in the structure of synthetic saponites: effect on crystallinity. Am. Mineral. 99 (1), 109–116.
He, H.P., Ji, S.C., Tao, Q., Zhu, J.X., Chen, T.H., Liang, X.L., Li, Z.H., Dong, H.L., 2017. Transformation of halloysite and kaolinite into beidellite under hydrothermal condition. Am. Mineral. 102 (6), 997–1005.
Inoue, A., Velde, B., Meunier, A., Touchard, G., 1988. Mechanism of illite formation during smectite-to-illite conversion in a hydrothermal system. Am. Mineral. 73 (11−12), 1325–1334.
Ji, S.C., Zhu, J.X., He, H.P., Tao, Q., Zhu, R.L., Ma, L.Y., Chen, M., Li, S.Y., Zhou, J.M., 2018. Conversion of serpentine to smectite under hydrothermal condition: Implication for solid-state transformation. Am. Mineral. 103 (2), 241–251.
Khodja, M., Canselier, J.P., Bergaya, F., Fourar, K., Khodja, M., Cohaut, N., Benmounah, A., 2010. Shale problems and water-based drilling fluid optimisation in the Hassi Messaoud Algerian oil field. Appl. Clay Sci. 49 (4), 383–393.
Kloprogge, J.T., 2006. Spectroscopic studies of synthetic and natural beidellites: a review. Appl. Clay Sci. 31 (3–4), 165–179.
Kloprogge, J.T., Jansen, J.B.H., Geus, J.W., 1990. Characterization of synthetic Na-beidellite. Clay Clay Miner. 38 (4), 409–414.
Kloprogge, J.T., Vandereerden, A.M.J., Jansen, J.B.H., Geus, J.W., Schuiling, R.D., 1993. Synthesis and paragenesis of Na-beidellite as a function of temperature, water-pressure, and sodium activity. Clay Clay Miner. 41 (4), 423–430.
Kloprogge, J.T., Hickey, L., Frost, R.L., 2000. The effect of increasing layer charge on the infrared absorption spectra of synthetic beidellites. J. Mater. Sci. Lett. 19 (13), 1131–1134.
Konta, J., 1995. Clay and man-clay raw-materials in the service of man. Appl. Clay Sci. 10 (4), 275–335.
Lindgreen, H., Jacobsen, H., Jakobsen, H.J., 1991. Diagenetic structural transformations in north-sea jurassic illite/smectite. Clay Clay Miner. 39 (1), 54–69.
Mackenzie, K.J.D., Brown, I.W.M., Cardile, C.M., Meinhold, R.H., 1987. The thermal-reactions of muscovite studied by high-resolution solid-state ^{29}Si and ^{27}Al NMR. J. Mater. Sci. 22 (7), 2645–2654.
van der Marel, H.W., Beutelspacher, H., 1976. Atlas of Infrared Spectroscopy of Clay Minerals and their Admixtures. Elsevier, Amsterdam.
Marumo, K., Hattori, K.H., 1999. Seafloor hydrothermal clay alteration at Jade in the back-arc Okinawa Trough: Mineralogy, geochemistry and isotope characteristics. Geochim. Cosmochim. Acta 63 (18), 2785–2804.
Mas, A., Guisseau, D., Mas, P.P., Beaufort, D., Genter, A., Sanjuan, B., Girard, J.P., 2006. Clay minerals related to the hydrothermal activity of the Bouillante geothermal field (Guadeloupe). J. Volcanol. Geotherm. Res. 158 (3–4), 380–400.
Mcmurtry, G.M., Yeh, H.W., 1981. Hydrothermal Clay mineral formation of East Pacific rise and Bauer basin sediments. Chem. Geol. 32 (3–4), 189–205.
Murakami, T., Sato, T., Inoue, A., 1999. HRTEM evidence for the process and mechanism of saponite-to-chlorite conversion through corrensite. Am. Mineral. 84 (7–8), 1080–1087.
Murray, H.H., Kogel, J.E., 2005. Engineered clay products for the paper industry. Appl. Clay Sci. 29 (3–4), 199–206.
Nagai, N., Ihara, K., Itoi, A., Kodaira, T., Takashima, H., Hakuta, Y., Bando, K.K., Itoh, N., Mizukami, F., 2012. Fabrication of boehmite and Al_2O_3 nonwovens from boehmite nanofibres and their potential as the sorbent. J. Mater. Chem. 22 (39), 21225–21231.
Noh, Y.D., Komarneni, S., Mackenzie, K.J.D., Ro, H.M., Park, M., 2013. Highly charged swelling micas of different charge densities: Synthesis, characterization, and selectivity for Sr and Ba. Sep. Purif. Technol. 104, 238–245.
Pavon, E., Castro, M.A., Naranjo, M., Orta, M.M., Pazos, M.C., Alba, M.D., 2013. Hydration properties of synthetic high-charge micas saturated with different cations: an experimental approach. Am. Mineral. 98 (23), 394–400.
Pazos, M.C., Castro, M.A., Orta, M.M., Pavon, E., Rios, J.S.V., Alba, M.D., 2012. Synthetic high-charge organomica: effect of the layer charge and alkyl chain length on the structure of the adsorbed surfactants. Langmuir 28 (19), 7325–7332.
Pomakhina, E., Deneele, D., Gaillot, A.C., Paris, M., Ouvrard, G., 2012. ^{29}Si solid state NMR investigation of pozzolanic reaction occurring in lime-treated Ca-bentonite. Cem. Concr. Res. 42 (2), 626–632.
Ram, S., 2001. Infrared spectral study of molecular vibrations in amorphous, nanocrystalline and $AlO(OH)\cdot\alpha H_2O$ bulk crystals. Infrared Phys. Technol. 42 (6), 547–560.
Sanz, J., Serratosa, J.M., 1984. ^{29}Si and ^{27}Al high-resolution MAS-NMR spectra of phyllosilicates. J. Am. Chem. Soc. 106 (17), 4790–4793.
Srodon, J., 1980. Synthesis of mixed-layer kaolinite-smectite. Clay Clay Miner. 28 (6), 419–424.
Srodon, J., Eberl, D.D., 1984. Illite. Rev. Mineral. 13, 495–544.
Trolard, F., Tardy, Y., 1987. The stabilities of gibbsite, boehmite, aluminous goethites and aluminous hematites in bauxites, ferricretes and laterites as a function of water activity, temperature and particle-size. Geochim. Cosmochim. Acta 51 (4), 945–957.
Viseras, C., Cerezo, P., Sanchez, R., Salcedo, I., Aguzzi, C., 2010. Current challenges in clay minerals for drug delivery. Appl. Clay Sci. 48 (3), 291–295.
Wolfenden, E.B., 1965. Geochemical behaviour of trace elements during bauxite formation in Sarawak Malaysia. Geochim. Cosmochim. Acta 29 (9), 1051–1062.
Yanagisawa, K., Kusunose, T., Ioku, K., Yamasaki, N., Malla, P.B., Komarneni, S., 1995. Hydrothermal crystallization mechanism of sodium beidellite from amorphous gel. J. Mater. Sci. Lett. 14 (24), 1770–1772.
Yu, W.C., Wang, R.H., Zhang, Q.L., Du, Y.S., Chen, Y., Liang, Y.P., 2014. Mineralogical and geochemical evolution of the Fusui bauxite deposit in Guangxi, South China: from the original Permian orebody to a Quarternary Salento-type deposit. J. Geochem. Explor. 146, 75–88.
Zhang, D., Zhou, C.H., Lin, C.X., Tong, D.S., Yu, W.H., 2010. Synthesis of clay minerals. Appl. Clay Sci. 50 (1), 1–11.
Zhu, R.L., Chen, Q.Z., Zhou, Q., Xi, Y.F., Zhu, J.X., He, H.P., 2016. Adsorbents based on montmorillonite for contaminant removal from water: a review. Appl. Clay Sci. 123, 239–258.